

Simultaneous Enhancement in the Electrical Conductivity and Reduction in the Lattice Thermal Conductivity Leading to Enhanced Thermoelectric ZT Realized by Incorporation of Metallic Nanoparticles into Oxide Matrix

Hirata, Shinji

Department of Applied Science for Electronics and Materials, Interdisciplinary Graduate School of Engineering Sciences, Kyushu University

Ohtaki, Michitaka

Department of Applied Science for Electronics and Materials, Interdisciplinary Graduate School of Engineering Sciences, Kyushu University

<https://doi.org/10.5109/2740934>

出版情報 : Evergreen. 7 (1), pp.1-6, 2020-03. 九州大学グリーンテクノロジー研究教育センターバージョン :

権利関係 : Creative Commons Attribution-NonCommercial 4.0 International



Simultaneous Enhancement in the Electrical Conductivity and Reduction in the Lattice Thermal Conductivity Leading to Enhanced Thermoelectric ZT Realized by Incorporation of Metallic Nanoparticles into Oxide Matrix

Shinji Hirata¹, Michitaka Ohtaki^{1, 2, *}

¹ Department of Applied Science for Electronics and Materials, Interdisciplinary Graduate School of Engineering Sciences, Kyushu University, Japan

² Transdisciplinary Research and Education Center for Green Technologies, Kyushu University, Japan

*Corresponding author, E-mail: ohtaki@kyudai.jp

(Received March 9, 2020; Received March 27, 2020; accepted March 27, 2020).

Abstract: Nanoporous Fe_3O_4 composites containing metallic Cu nanoparticles were synthesized by reducing-leaching treatment of CuFe_2O_4 precursor. Thermoelectric properties of the composites sintered at 1270 °C greatly improved compared with Fe_3O_4 without Cu, presumably due to a nanoporous structure and the Cu nanoparticles remaining in the Fe_3O_4 matrix after acid leaching. The electrical and thermal conductivity indicate that Cu in the matrix promotes the electron conduction and suppresses the phonon conduction, improving the dimensionless figure-of-merit, ZT .

Keywords: thermoelectrics; nanocomposites; metallic nanoparticles; nanoporous structure; phonon scattering; oxides

1. Introduction

Global energy consumption increasing year by year requires a technique development of renewable energy source such as wind and solar energy.¹⁻²⁾ Thermoelectrics, a class of materials utilized to convert heat directly into electricity by the Seebeck effect, is also expected to be another source of renewable energy. Thermoelectric materials are evaluated by the dimensionless figure-of-merit,

$$ZT = \frac{S^2 \sigma}{\kappa} T = \frac{S^2 \sigma}{\kappa_{\text{el}} + \kappa_{\text{ph}}} T, \quad (1)$$

where σ is the electrical conductivity, S is the Seebeck coefficient, T is the absolute temperature, κ is the thermal conductivity, κ_{el} is the electron thermal conductivity, and κ_{ph} is the phonon thermal conductivity. Good thermoelectric materials should have high σ and S with low κ simultaneously. However, σ , S and κ_{el} are all a function of the carrier concentration and hence interdependent each other, making good materials difficult to develop. On the other hand, κ_{ph} is associated with crystal lattice vibrations, and the only parameter insensitive to the carrier concentration, being independent of other parameters in ZT . Therefore, an approach to selectively decrease κ_{ph} is one of the most prospective way to improve ZT .³⁻²⁰⁾

Recent studies showed that nanostructure control in

materials is an efficient way to decrease the phonon thermal conductivity.²¹⁾ Coarse porous structure can decrease κ , while σ is also suppressed equally or more strongly due to the reduction of the cross-sectional area for the electron conduction.²²⁾ Meanwhile, nanocomposite structure can selectively reduce κ , specifically κ_{ph} , because of phonon scattering by nanopores and nanoparticles.²³⁾ This specific decrease in κ_{ph} is governed by the composite structure, particularly the size of the pore and the particles.

In this paper, we report novel synthesis of nanoporous oxide containing metallic nanoparticles and investigation of a relation between the structure and the thermoelectric properties of the oxide composites. A copper spinel CuM_2O_4 ($M = \text{Fe, Al, Mn, Ni}$) has been reported to form metallic Cu nanoparticles in M -oxide matrix by heating in a reducing atmosphere.²⁴⁻²⁶⁾ If the Cu nanoparticles in the matrix can be selectively removed, nanosized pores will remain in the oxide. Here, we focused on CuFe_2O_4 , which is expected to form Fe_3O_4 composite containing Cu nanoparticles after H_2 reduction, because the iron oxide is more electrically conductive than aluminum or manganese oxides to be obtained as a matrix by reducing CuAl_2O_4 and CuMn_2O_4 . Finally, we aim to establish an innovative nanostructure-control approach to achieve high thermoelectric performance.

2. Experimental

2.1 Sample preparation

CuFe_2O_4 , a precursor of the nanocomposites was prepared by calcining a mixed powder of $\alpha\text{-Fe}_2\text{O}_3$ (99%, Kishida Kagaku) and CuO (99.9%, Wako) at 1000 °C for 4 h in air. The copper spinel oxide thus formed was ground in a mortar and heated in a reducing atmosphere (5% H_2/N_2) at 270 °C for 14h. After the reduction, the sample powder was washed with 69% nitric acid for leaching of metallic copper. The reducing and leaching processes (denoted as R-L cycle hereafter) were repeated under the same conditions for some samples. These powders were finally sintered at 1270 °C for 3 h in an N_2 atmosphere. For comparison, a reagent grade Fe_3O_4 (95%, Wako) was also sintered under the same conditions.

2.2 Characterization

Powder x-ray diffraction (XRD) measurements were performed using a PANalytical EMPYREAN diffractometer with $\text{Cu-K}\alpha$ radiation. The surface structures of the samples were observed on a scanning electron microscope (SEM, Hitachi S-4800). The amount of copper and iron after each treatment were determined by inductively coupled plasma-optical emission spectroscopy (ICP-OES, Jobin Yvon Horiba, ULTIMA 2C). The thermal conductivity was obtained from the thermal diffusivity and the specific heat measured on a Kyoto Electronics LFA-502 laser flash measurement system and a Netzsch DSC404F3 Pegasus, respectively. The electrical conductivity and the Seebeck coefficient were measured under Ar atmosphere simultaneously on an Ozawa Science RZ2001i apparatus.

3. Results and Discussion

3.1 Nanocomposite Structure

Figure 1 shows the XRD patterns of the copper ferrites after each treatment. These patterns indicate that the precursor consisted mainly of CuFe_2O_4 (Fig. 1(a)), and

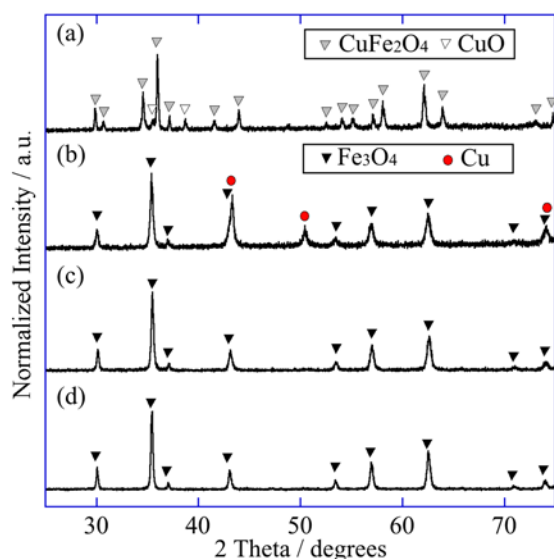


Fig. 1: XRD patterns of CuFe_2O_4 (a) before and (b) after reduction, (c) after reduction and leaching for 1 and (d) 5 times.

Table 1. The Cu amount in the samples after each treatment relative to the nominal Cu amount in CuFe_2O_4 .

Treatment	Relative Cu amount / CuFe_2O_4 u.f.
only reduction	1.03
1 R-L cycle	0.20
3 R-L cycle	0.13
5 R-L cycle	0.11

metallic Cu and Fe_3O_4 formed after the reduction (Fig. 1(b)). After leaching with 69% HNO_3 , the Cu peaks at 43.3, 50.4 and 74.1° disappeared (Fig. 1(c)). These results demonstrate that 69% nitric acid can preferentially remove the metallic Cu from the reduced CuFe_2O_4 leaving Fe_3O_4 as a matrix. Table 1 summarizes the results of ICP-OES analysis for the samples. The amount of Cu in the samples after the reducing-leaching (R-L) cycles of 1 and 5 times decreased to 20 % and 11% of the initially charged Cu, respectively. These results suggest that the copper amount remaining in the Fe_3O_4 matrix can be controlled by the R-L cycles.

Figure 2 shows the surfaces of the samples after each treatment. Whereas the surface of the copper spinel before the reduction is dense and smooth (Fig. 2(a)), a number of Cu nanoparticles were observed on the surface of the reduced CuFe_2O_4 (Fig. 2(b)). A nanoporous structure formed after leaching Cu nanoparticles (Fig. 2(c)), and the pore diameter was similar to the size of the Cu nanoparticles observed prior to the leaching treatment. These results indicate that the nanoporous structure was formed by selective leaching of copper nanoparticles from the reduced CuFe_2O_4 . After the R-L cycles for 5 times, the pore size increased, from 50 nm to more than 100 nm (Fig. 2(d)).

These observation suggests that the structural transformation proceeds as depicted in Fig. 3. The nanoporous

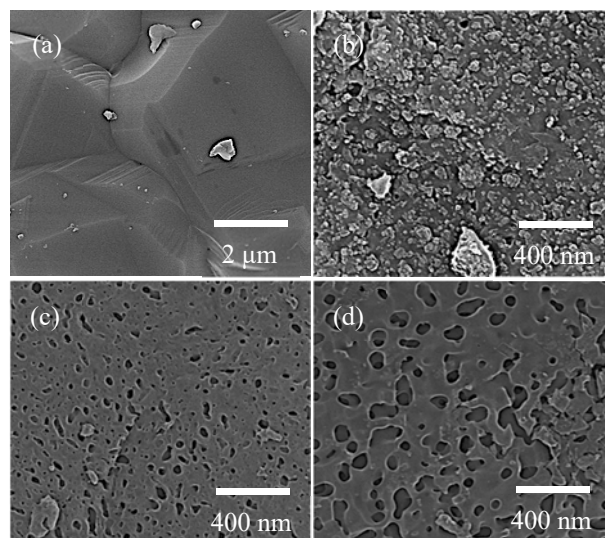


Fig. 2: SEM images of CuFe_2O_4 (a) before and (b) after reduction, (c) after reduction and leaching for 1 and (d) for 5 times.

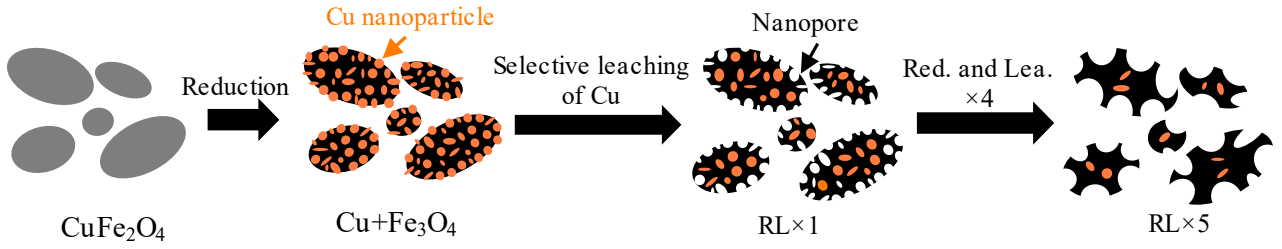


Fig. 3: Schematic diagram for synthesis of nanoporous Fe₃O₄ containing Cu nanoparticles.

Fe₃O₄ composite powders containing Cu nanoparticles were thereby synthesized by selective leaching of the Cu nanoparticles from the reduced CuFe₂O₄.

3.2 Thermoelectric properties

In order to investigate thermoelectric properties of the Fe₃O₄ nanocomposites thus obtained, we sintered the nanocomposite powders at 1270 °C in N₂. Sintered bodies of the Fe₃O₄ nanocomposites after 1 and 5 R-L cycles will be denoted as 1RL and 5RL, respectively. Fe₃O₄ represents the reagent grade Fe₃O₄ sintered under the same conditions. The relative densities of 1RL, 5RL, and Fe₃O₄ were 96, 94, and 99%, respectively. The nanoporous structure disappeared from the surface of the sintered bodies (Fig. 4), while the main phase of the samples remained Fe₃O₄ with a small XRD peak of Cu at 2θ = 50.4 ° (Fig. 5), being consistent with the ICP results (Table 1). Therefore, it is plausible that the Cu nanoparticles

remaining in the Fe₃O₄ matrix would influence the thermoelectric properties.

Figure 6 shows the temperature dependence of the electrical conductivity, σ . All the samples exhibited the semiconducting behavior, in which σ increases with increasing temperature. The σ values of 1RL and 5RL were about 10 times higher than that of Fe₃O₄ without Cu. Since the CuFe₂O₄ phase is much less conductive ($\sim 10^{-1}$ S cm⁻¹ at 300 °C) than Fe₃O₄,²⁷⁾ even if CuFe₂O₄ remained in the samples, it cannot rationalize the much higher σ of 1RL and 5RL. Therefore, only possible reason of the markedly increased σ would be the metallic Cu nanoparticles remaining in the Fe₃O₄ matrix. Figure 7 shows the temperature dependence of the Seebeck coefficient, S , which was almost the same for all the samples. This implies that the Cu nanoparticles remaining in the matrix has negligible influence on S .

The electrical conductivity, σ , is given by the following equation:

$$\sigma = ne\mu, \quad (2)$$

where n , e , and μ are the carrier concentration, electrical charge of the carrier, and the carrier mobility, respectively. For degenerate semiconductors, the Seebeck coefficient is given by:

$$S = \frac{8\pi^2 k_B^2}{3eh^2} m^* T \left(\frac{\pi}{3n} \right)^{2/3} \propto n^{-2/3} \quad (3)$$

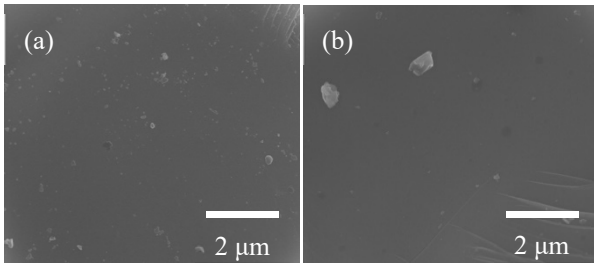


Fig. 4: SEM images of the surfaces of (a) 1 RL and (b) 5RL.

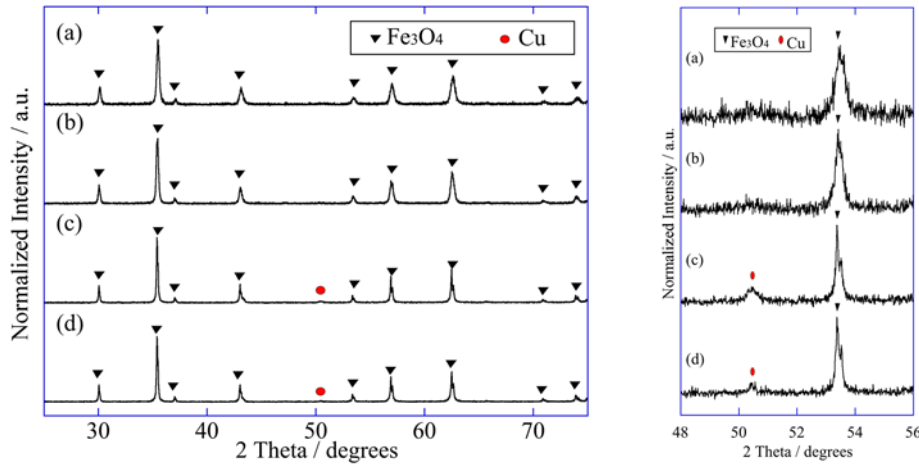


Fig. 5: XRD patterns for 1RL and 5RL (a, b) before and (c, d) after sintering.

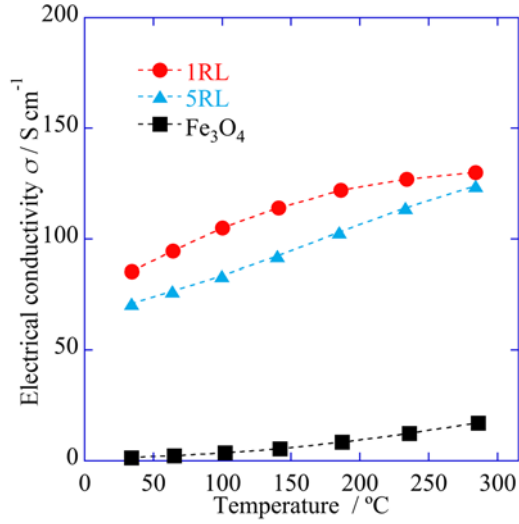


Fig. 6: Temperature dependence of the electrical conductivity of the samples.

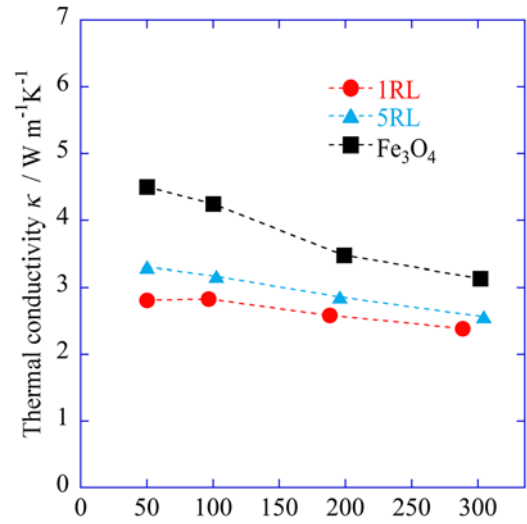


Fig. 8: Temperature dependence of the thermal conductivity of the samples.

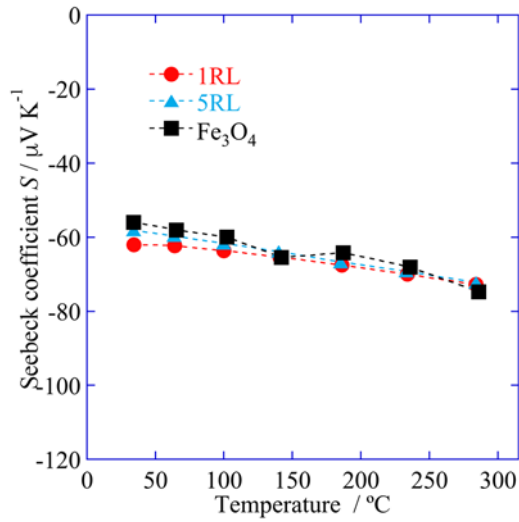


Fig. 7: Temperature dependence of the Seebeck coefficient of the samples.

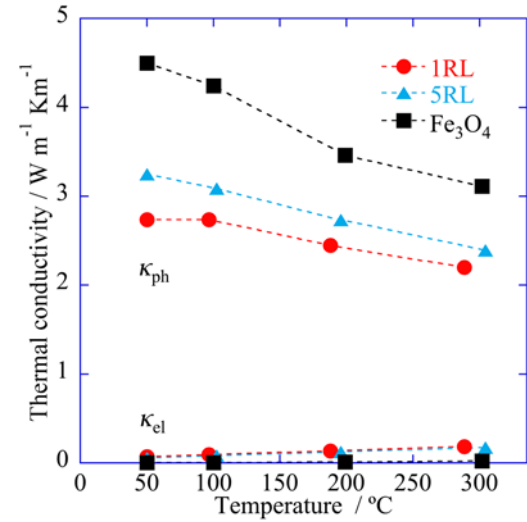


Fig. 9: Temperature dependence of the electron and phonon thermal conductivity of the samples.

where k_B , h , and m^* are the Boltzmann constant, the Plank constant, and the effective mass of the carrier, respectively. These equations show that σ and S are oppositely dependent on n , while our results are inconsistent with this relation. It is therefore implied that the Cu nanoparticles provide an additional conduction path with higher carrier mobility, giving negligible influence on the overall carrier concentration.

Figure 8 shows the temperature dependence of the thermal conductivity of the samples. The thermal conductivity of the samples containing Cu was significantly lower than that of the Cu-free Fe_3O_4 . Moreover, the more Cu remained in the samples, the more κ decreased. To investigate the carrier and phonon thermal conduction, we calculated the electron thermal conductivity, κ_{el} , and the phonon thermal conductivity, κ_{ph} , using the following equations:

$$\kappa_{ph} = \kappa - \kappa_{el}, \quad (5)$$

where L_0 is the Lorentz number, $2.45 \times 10^{-8} \text{ V}^2 \text{ K}^{-2}$. Equation (4) is the Wiedemann-Franz law. Figure 9 shows the temperature dependence of κ_{el} and κ_{ph} of the samples. The electron thermal conductivity of all samples was very small. Although κ_{el} of 1RL and 5RL was slightly higher than that of Cu-free Fe_3O_4 , the maximum κ_{el} was just $0.20 \text{ W m}^{-1} \text{ K}^{-1}$ at 289°C for 1RL. On the other hand, κ_{ph} is strongly dependent on the Cu amount remaining after the leaching. The κ_{ph} values substantially decreased with increasing Cu amount, and the lowest κ_{ph} was obtained for 1RL containing 20% of initial amount of Cu. These results clearly indicated that the Cu nanoparticles remaining in the Fe_3O_4 matrix increased σ (and hence κ_{el}), and decreased κ_{ph} simultaneously, successfully decoupling electrical and thermal conduction.

In order to evaluate influence of the Cu nanoparticles on the thermoelectric properties, we have

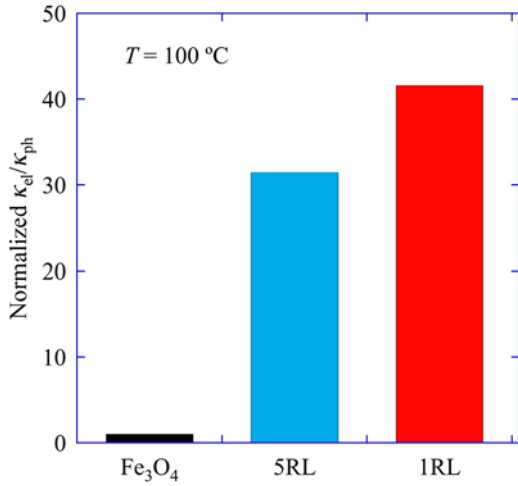


Fig. 10: The normalized $\kappa_{el} / \kappa_{ph}$ ratios of the samples at 100 °C.

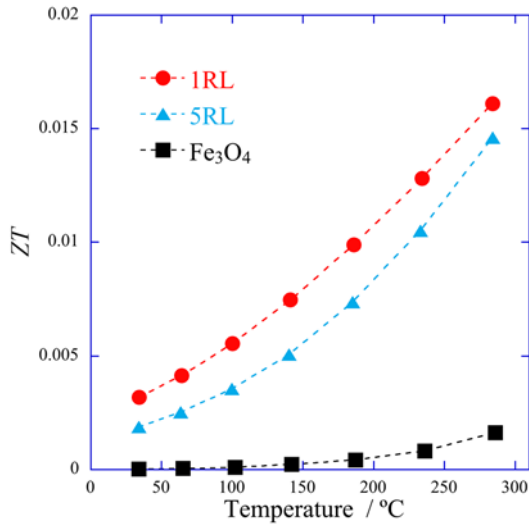


Fig. 11: Temperature dependence of dimensionless figure-of-merit of the samples.

examined a ratio κ_{el}/κ_{ph} as a quantitative measure. From eq. (1), (4) and (5), the definition of the dimensionless figure-of-merit, ZT , yields the following relation when $\kappa_{el} \ll \kappa_{ph}$:

$$ZT = \frac{S^2 \sigma T}{\kappa_{el} + \kappa_{ph}} = \frac{\frac{S^2}{L_0} T}{1 + \frac{\kappa_{ph}}{\kappa_{el}}} \sim \frac{S^2}{L_0} \frac{\kappa_{el}}{\kappa_{ph}}. \quad (6)$$

As shown in eq. (6), if $\kappa_{el} \ll \kappa_{ph}$ and S is almost unchanged, we can use the ratio, κ_{el}/κ_{ph} , as an indicator of selective phonon scattering or decoupling of the electron and phonon conduction. Figure 10 compares the κ_{el}/κ_{ph} ratios at 100 °C normalized by that of Fe₃O₄, and indicates that the samples containing the Cu nanoparticles have more than 30 times larger κ_{el}/κ_{ph} . It is therefore presumable that the Cu nanoparticles in the Fe₃O₄ matrix can simultaneously enhance the electron conduction and suppress the phonon conduction.

Figure 11 shows the temperature dependence of the dimensionless figure-of-merit of the samples. The highest ZT value of 1.57×10^{-2} at 284 °C obtained for 1RL was 10 times larger than that of Fe₃O₄. The normalized κ_{el}/κ_{ph} ratio of 1RL at 284 °C was 11.4, confirming that the prediction by eq. (6) is in good accordance with the observed increase in ZT . Since the relative density, d_{rel} , of the sintered samples were all more than 94%, and κ_{ph} was substantially lower for 1RL with $d_{rel} = 96\%$ than that of 5RL with $d_{rel} = 94\%$, the relative density or porosity of the samples is unable to rationalize the large difference in κ_{ph} . The most plausible explanation would be the fact that 1RL contained 20% of initial amount of Cu presumably as nanoparticles, which increased σ by providing a favorable conduction path and decreased κ_{ph} by enhancing phonon scattering simultaneously. It is hence strongly suggested that optimization of the amount of the Cu nanoparticles enables us to improve the thermoelectric properties of the oxide further. Moreover, if the nanoporous structure of the powders after the R-L cycles can be preserved during sintering, the thermal conductivity would further decrease, improving ZT furthermore.

4. Conclusions

Nanoporous Fe₃O₄ composite powders containing Cu nanoparticles were synthesized by selective leaching of the Cu nanoparticles from reduced CuFe₂O₄ matrix. The porous structure and the amount of Cu remaining in the Fe₃O₄ matrix can be controlled by reducing-leaching cycles. After sintering, the porous structure disappeared, whereas the left-over Cu nanoparticles improve the thermoelectric properties. The more Cu remained in the Fe₃O₄ matrix, the higher electrical conductivity and the lower thermal conductivity were obtained. These results suggested that the Cu nanoparticles remaining in the Fe₃O₄ improved the thermoelectric properties by the provision of carrier conduction path and the enhancement of phonon scattering, making the ZT about 10 times higher than that of the Fe₃O₄ without Cu. Furthermore, all the results mean that we therefore established nanostructure-control approach to increase electrical conductivity and decrease thermal conductivity simultaneously. We can expect an introduction of nanocomposite structure to some good thermoelectric materials such as SrTiO₃ and ZnO by using this approach, and improve their thermoelectric properties further.

Acknowledgements

The authors would like to thank Assoc. Prof. K. Suekuni and Assist. Prof. K. Watanabe for their valuable discussion, and Fukuoka Industrial Technology Center for XRD measurement and SEM observation.

This work was financially supported by JSPS KAKENHI Grant Number JP19H02800.

References

- 1) A.M.M. Ismaiel, S.M. Metwalli, B.M.N. Elhadidi, and S. Yoshida, *Evergreen*, **4**, 1 (2017).
- 2) P. Pal, A.K. Nayak, and R. Dev, *Evergreen*, **5**, 52 (2018).
- 3) C.J. Vineis, A. Shakouri, A. Majumdar, and M.G. Kanatzidis, *Adv. Mater.*, **22**, 3970 (2010).
- 4) B. Xu, T. Feng, M.T. Agne, L. Zhou, X. Ruan, G.J. Snyder, and Y. Wu, *Angew. Chemie - Int. Ed.*, **56**, 3546 (2017).
- 5) K. Biswas, J. He, Q. Zhang, G. Wang, C. Uher, V.P. Dravid, and M.G. Kanatzidis, *Nat. Chem.*, **3**, 160 (2011).
- 6) K. Biswas, J. He, I.D. Blum, C.I. Wu, T.P. Hogan, D.N. Seidman, V.P. Dravid, and M.G. Kanatzidis, *Nature*, **489**, 414 (2012).
- 7) T. Mori, *Small*, **13**, 1 (2017).
- 8) G. Joshi, H. Lee, Y. Lan, X. Wang, G. Zhu, D. Wang, R.W. Gould, D.C. Cuff, M.Y. Tang, M.S. Dresselhaus, G. Chen, and Z. Ren, *Nano Lett.*, **8**, 4670 (2008).
- 9) B. Poudel, Q. Hao, Y. Ma, Y. Lan, A. Minnich, B. Yu, X. Yan, D. Wang, A. Muto, D. Vashaee, X. Chen, J. Liu, M.S. Dresselhaus, G. Chen, and Z. Ren, *Science*, **320**, 634 (2008).
- 10) G. Rogl, A. Grytsiv, P. Rogl, N. Peranio, E. Bauer, M. Zehetbauer, and O. Eibl, *Acta Mater.*, **63**, 30 (2014).
- 11) G. Rogl, A. Grytsiv, K. Yubuta, S. Puchegger, E. Bauer, C. Raju, R.C. Mallik, and P. Rogl, *Acta Mater.*, **95**, 201 (2015).
- 12) S. Grasso, N. Tsujii, Q. Jiang, J. Khaliq, S. Maruyama, M. Miranda, K. Simpson, T. Mori, and M.J. Reece, *J. Mater. Chem. C*, **1**, (12) 2362 (2013).
- 13) L. Hu, T. Zhu, X. Liu, and X. Zhao, *Adv. Funct. Mater.*, **24**, 5211 (2014).
- 14) L.P. Hu, T.J. Zhu, Y.G. Wang, H.H. Xie, Z.J. Xu, and X.B. Zhao, *NPG Asia Mater.*, **6**, 1 (2014).
- 15) Z.J. Xu, L.P. Hu, P.J. Ying, X.B. Zhao, and T.J. Zhu, *Acta Mater.*, **84**, 385 (2015).
- 16) J. He, J.R. Sootsman, S.N. Girard, J.C. Zheng, J. Wen, Y. Zhu, M.G. Kanatzidis, and V.P. Dravid, *J. Am. Chem. Soc.*, **132**, 8669 (2010).
- 17) J.F. Li, W.S. Liu, L.D. Zhao, and M. Zhou, *NPG Asia Mater.*, **2**, 152 (2010).
- 18) C. Nethravathi, C.R. Rajamathi, M. Rajamathi, R. Maki, T. Mori, D. Golberg, and Y. Bando, *J. Mater. Chem. A*, **2**, 985 (2014).
- 19) X. Shi, J. Yang, J.R. Salvador, M. Chi, J.Y. Cho, H. Wang, S. Bai, J. Yang, W. Zhang, and L. Chen, *J. Am. Chem. Soc.*, **133**, 7837 (2011).
- 20) T. Liang, X. Su, Y. Yan, G. Zheng, Q. Zhang, H. Chi, X. Tang, and C. Uher, *J. Mater. Chem. A*, **2**, 17914 (2014).
- 21) M.G. Kanatzidis, *Chem. Mater.*, **22**, 648 (2010).
- 22) M. Ohtaki, and K. Araki, *J. Ceram. Soc. Japan*, **119**, 813 (2011).
- 23) H. Machraf, and G. Lebon, *Phys. Lett. Sect. A Gen. At. Solid State Phys.*, **379**, 968 (2015).
- 24) Y.H. Huang, S.F. Wang, A.P. Tsai, and S. Kameoka, *Ceram. Int.*, **40**, 4541 (2014).
- 25) S. Kameoka, T. Tanabe, and A.P. Tsai, *J. Ceram. Soc. Japan*, **22**, 138 (2010).
- 26) Y.H. Huang, S.F. Wang, A.P. Tsai, and S. Kameoka, *J. Power Sources*, **281**, 138 (2015).
- 27) A.I. Eatah, A.A. Ghani, and E. El Faramawy, *Phys. Status Solidi*, **105**, 231 (1988).